

# Tightly bound trions in monolayer MoS<sub>2</sub>

Kin Fai Mak<sup>1</sup>, Keliang He<sup>2</sup>, Changgu Lee<sup>3</sup>, Gwan Hyoung Lee<sup>4</sup>, James Hone<sup>4</sup>, Tony F. Heinz<sup>1</sup>  
and Jie Shan<sup>2\*</sup>

**Two-dimensional (2D) atomic crystals, such as graphene and transition-metal dichalcogenides, have emerged as a new class of materials with remarkable physical properties<sup>1</sup>. In contrast to graphene, monolayer MoS<sub>2</sub> is a non-centrosymmetric material with a direct energy gap<sup>2–5</sup>. Strong photoluminescence<sup>2,3</sup>, a current on/off ratio exceeding 10<sup>8</sup> in field-effect transistors<sup>6</sup>, and efficient valley and spin control by optical helicity<sup>7–9</sup> have recently been demonstrated in this material. Here we report the spectroscopic identification in a monolayer MoS<sub>2</sub> field-effect transistor of tightly bound negative trions, a quasiparticle composed of two electrons and a hole. These quasiparticles, which can be optically created with valley and spin polarized holes, have no analogue in conventional semiconductors. They also possess a large binding energy (~20 meV), rendering them significant even at room temperature. Our results open up possibilities both for fundamental studies of many-body interactions and for optoelectronic and valleytronic applications in 2D atomic crystals.**

The trion binding energy that we observe in monolayer MoS<sub>2</sub> is nearly an order of magnitude larger than that found in conventional quasi-2D systems, such as semiconductor quantum wells<sup>10–13</sup>. This is a consequence of the greatly enhanced Coulomb interactions in monolayer MoS<sub>2</sub>, arising from reduced dielectric screening in gapped 2D crystals and the relatively heavy particle band masses associated with the Mo *d*-manifolds<sup>4,5,14</sup>. For an electron density as high as  $n = 10^{11} \text{ cm}^{-2}$ , for instance, the dimensionless interaction parameter  $r_s$  is  $\sim 60$  in monolayer MoS<sub>2</sub> (Supplementary Section S1). This value is significantly larger than that for carriers in quantum wells even at very low doping levels<sup>15</sup>. Monolayer MoS<sub>2</sub> is a strongly interacting system even in the presence of relatively high carrier densities; it thus presents an ideal laboratory for exploring many-body phenomena, such as carrier multiplication and Wigner crystallization<sup>16</sup>.

The atomic structure of MoS<sub>2</sub> consists of hexagonal planes of S and Mo atoms in a trigonal prismatic structure (Fig. 1a; ref. 17). The two sublattices of the hexagonal MoS<sub>2</sub> structure are occupied, respectively, by one Mo and two S atoms (Fig. 1b). Monolayer MoS<sub>2</sub> is a direct gap semiconductor with energy gaps located at the K and K' points of the Brillouin zone (Fig. 1c). Both the highest valence bands and the lowest conduction bands are formed primarily from the Mo *d*-orbitals<sup>4,17</sup>. The large spin-orbit interaction splits the highest valence bands at the K (K') point by  $\sim 160 \text{ meV}$  (refs 2,3,7). The valley and spin degrees are coupled because of the lack of inversion symmetry in monolayer MoS<sub>2</sub> (ref. 18). As has been recently shown experimentally, this allows optical pumping of a single valley (and spin) with circularly polarized light<sup>7–9</sup>.

Here we investigate the optical response of monolayer MoS<sub>2</sub> as a function of carrier density by means of absorption and

photoluminescence spectroscopy. In our investigations we have made use of MoS<sub>2</sub> monolayers prepared by mechanical exfoliation. Field-effect transistors (FETs) using MoS<sub>2</sub> were fabricated on SiO<sub>2</sub>/Si substrates; the doping density in the MoS<sub>2</sub> channel was systematically varied by applying a voltage to the Si back gate. All measurements were performed at 10 K, if not otherwise specified. The typical variation of the drain–source current ( $I_{ds}$ ) with the gate voltage ( $V_g$ ) is shown in the inset of Fig. 1d. The response is characteristic of a FET with an *n*-type channel. Spontaneous negative doping, presumably from defects within the MoS<sub>2</sub> layer and/or substrate interactions, has been commonly reported in mechanically exfoliated MoS<sub>2</sub> (refs 6,19). Over the accessible range of the gate voltage (–100 to +80 V) our MoS<sub>2</sub> FETs exhibit electron doping. The low off-state current at high negative gate voltages is understood to reflect electron localization in 2D (ref. 15) and/or a channel-contact barrier.

The absorption spectrum of monolayer MoS<sub>2</sub> at a gate voltage of –100 V (Fig. 1d) corresponds to that of a nearly undoped sample. It shows pronounced absorption peaks from excitonic transitions, rather than the steps that would be expected for absorption arising from band-to-band transitions in 2D. The two features, known as the A ( $\sim 1.92 \text{ eV}$ ) and B ( $\sim 2.08 \text{ eV}$ ) excitons<sup>2,3,20</sup>, are associated with direct optical transitions from the highest spin-split valence bands to the lowest conduction bands. These transitions are significantly modified by strong Coulomb interactions between the photogenerated electron–hole pairs and the corresponding formation of bound excitons.

In our investigation of the optical response of MoS<sub>2</sub> in the presence of a 2D electron gas (2DEG), we focus on the behaviour of the low-energy (A) exciton over the spectral range of 1.8–2.0 eV. Figure 2a (red lines) shows representative absorption spectra of a monolayer MoS<sub>2</sub> FET under gate voltages from –100 to 80 V, corresponding to approximate charge neutrality to a doping density of  $\sim 10^{13} \text{ cm}^{-2}$ . We see an overall suppression of the optical absorbance in this spectral region with increasing electron doping. The prominent A exciton peak evolves into two resonances, with the emergence of a lower energy resonance (labelled as A<sup>–</sup>). For  $V_g > 0$ , the absorbance of feature A diminishes rapidly and disappears into the background. The A<sup>–</sup> feature, on the other hand, broadens gradually, while approximately preserving its spectral weight. Similarly, in the photoluminescence spectra (Fig. 2a), both resonances can be identified for negative gate voltages. The photoluminescence intensity of the A exciton, like its absorbance, can be switched off by doping. In addition, redshifts in the photoluminescence peak energies from the corresponding absorption energies (Stokes shifts) are observed for both features; the magnitude of Stokes shift is found to increase with doping level (Supplementary Fig. S1b).

<sup>1</sup>Departments of Physics and Electrical Engineering, Columbia University, 538 West 120th Street, New York 10027, USA, <sup>2</sup>Department of Physics, Case Western Reserve University, 10900 Euclid Avenue, Cleveland, Ohio 44106, USA, <sup>3</sup>SKKU Advanced Institute of Nanotechnology (SAINT) and Department of Mechanical Engineering, Sungkyunkwan University, Suwon 440-746, Korea, <sup>4</sup>Department of Mechanical Engineering, Columbia University, New York 10027, USA. \*e-mail: jie.shan@case.edu.

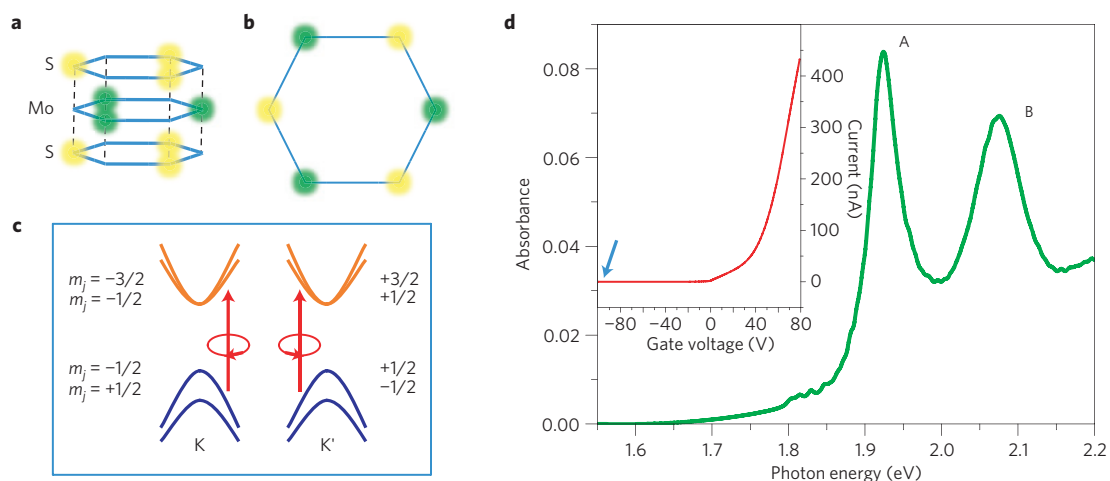


**Figure 1 | Atomic structure, electronic band structure, and absorption spectrum of monolayer MoS<sub>2</sub>.** **a**, Representation of the trigonal prismatic structure of monolayer MoS<sub>2</sub>. **b**, Honeycomb lattice structure with each sublattice occupied by a Mo and two S atoms. **c**, The lowest-energy conduction bands and the highest-energy valence bands labeled by the z-component of their total angular momentum near the K and K' point of the Brillouin zone. The spin degeneracy at the valence-band edges is lifted by spin-orbit interactions. The valley and spin degrees of freedom are coupled. Under left-circularly polarized excitation, only the K-valley is populated, whereas under right-circularly polarized excitation, only the K'-valley is populated. **d**, Absorption spectrum of undoped monolayer MoS<sub>2</sub> with two prominent resonances, known as the A and B excitons. The inset shows the drain-source current  $I_{ds}$ , under a  $V_{ds} = 40$  mV bias voltage, as a function of back-gate voltage  $V_g$ . It is characteristic of an n-doped semiconductor that can be turned off at large negative gate voltages.

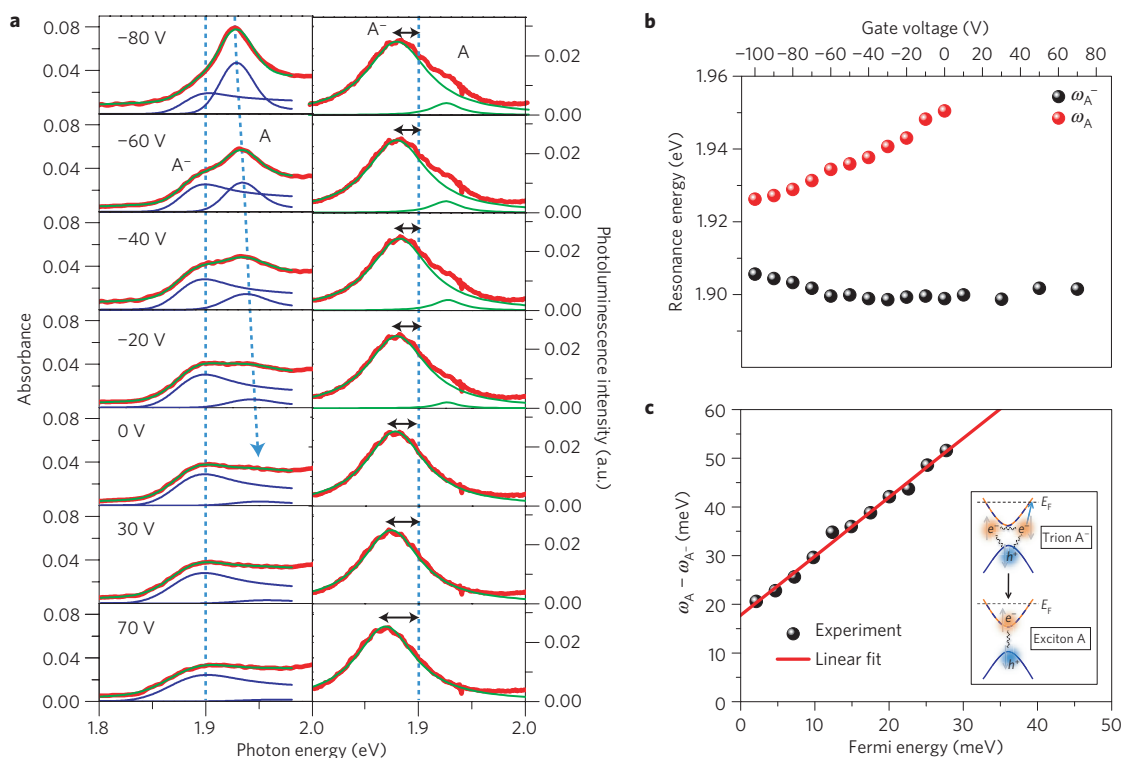


**Figure 2 | Doping dependence of the optical properties of a monolayer MoS<sub>2</sub> FET.** **a**, Absorption and photoluminescence spectra (red lines) in the range of 1.8–2.0 eV for the indicated back-gate voltages. The exciton (A) and trion ( $A^-$ ) resonances behave differently with gate voltage. Left: Absorption spectra, with the dashed blue lines as a guide to the eye for the threshold energies of A and  $A^-$  features. The green lines are power-law fits to the experimental results, as described in the main text, with the A and  $A^-$  components shown as the blue lines. Right: The photoluminescence spectra of the A and  $A^-$  features are fit to Lorentzians (green lines). The dashed blue line indicates the absorption peak of the  $A^-$  resonance and the arrows show the doping-dependent Stokes shift of the trion photoluminescence. **b**, Threshold energies of the trion  $\omega_{A^-}$  (black symbols) and the neutral exciton  $\omega_A$  (red symbols), determined from the absorption spectra, as a function of gate voltage (upper axis) and Fermi energy  $E_F$  (lower axis). **c**, The difference in the exciton and trion energies,  $\omega_A - \omega_{A^-}$  (symbols), as a function of Fermi energy  $E_F$ . The red line, a linear fit to the  $E_F$ -dependence, has a slope of 1.2 and an intercept of 18 meV. The latter determines the trion binding energy. Inset: representation of the dissociation of a trion into an exciton and an electron at the Fermi level.

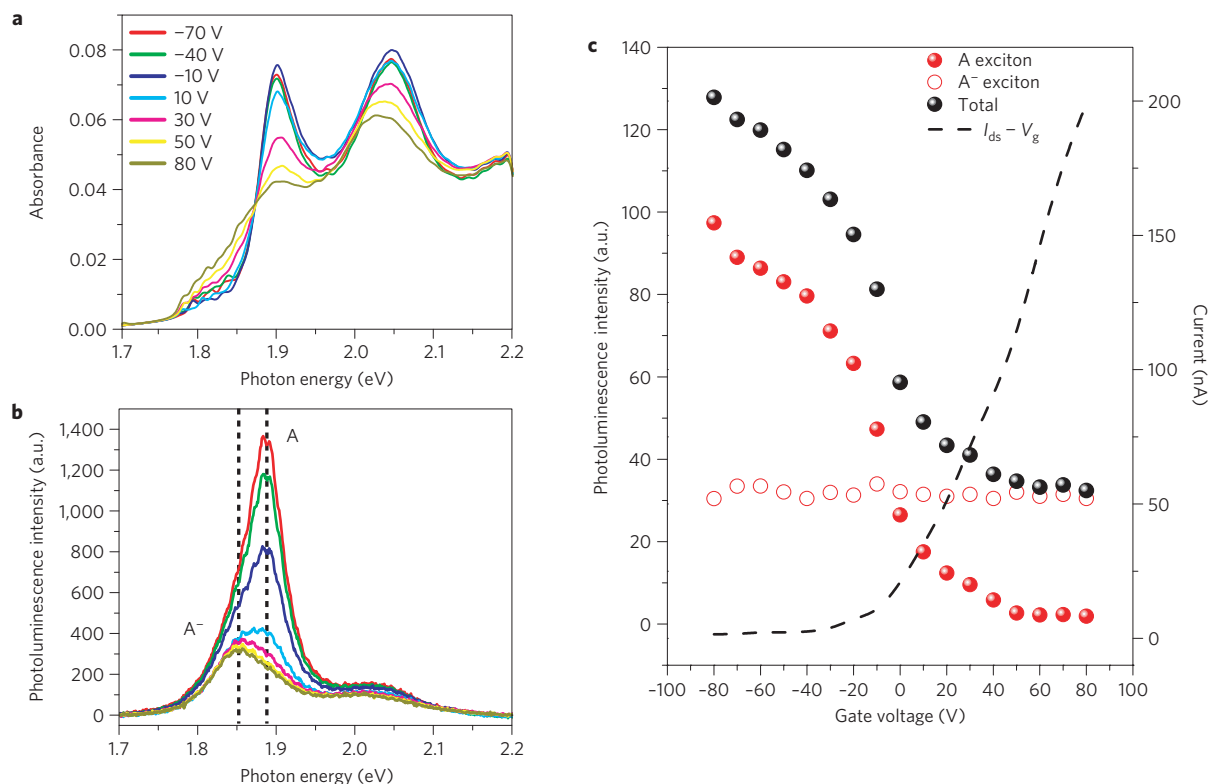


**Figure 3 | Excitons and trions at room temperature in monolayer MoS<sub>2</sub>.** **a, b**, Absorption and photoluminescence spectra at different back-gate voltages. Both the neutral exciton (A) and trion (A<sup>-</sup>) features (with the corresponding resonance energies indicated by the dashed lines) can be identified, although the resonances are significantly broadened. **c**, Dependence on gate voltage of the drain-source current (right) and the integrated photoluminescence intensity of the A and A<sup>-</sup> features and their total contribution (left).

What is the origin of the A<sup>-</sup> resonance? Our observation cannot be explained by a simple state-blocking effect. Although such Pauli blocking can account for the overall reduction in absorption with doping<sup>21</sup>, it cannot explain the appearance of two resonances with different doping dependences. Nor can the emergence of two features be explained by an electric-field-induced band structure modification. In the absence of magnetic fields, the valley and spin degeneracy of the bands is protected and no available degeneracy can be lifted to give rise to two distinct resonances. The observed A<sup>-</sup> feature, however, can be understood as arising from trions. Such bound states of two electrons to a hole, that is, negatively charged excitons, are known to have finite binding energies<sup>10,11,22,23</sup>. In our experiment at low temperature, the optical response of monolayer MoS<sub>2</sub> is dominated by neutral excitons in undoped samples. Trions emerge, accompanied by a reduction of exciton absorption and photoluminescence, when excess electrons are introduced to bind to photoexcited electron-hole pairs. The exciton spectral weight is transferred to the trion, as shown in our experiment. The detailed dependence on doping density of this phenomenon in the relatively low doping regime is often governed by electron localization in inhomogeneous samples.

We have analysed the absorption spectra to determine the energies to create both neutral excitons ( $\omega_A$ ) and trions ( $\omega_{A^-}$ ) as a function of the doping level. The analysis is based on a fitting procedure using the predicted power-law spectral dependence<sup>21,24</sup> of the features (see Methods for details)<sup>21,24</sup>. We also convert the gate voltage to the electron doping density ( $ne = CV_g$ ) using the back-gate capacitance of  $C = 1.2 \times 10^{-8} \text{ F cm}^{-2}$  and then to the Fermi energy ( $E_F = \hbar^2 \pi n / 2m_e e^2$ ) using an electron band mass of  $m_e = 0.35m_0$  (ref. 14), where  $m_0$  is the electron mass. Because of intrinsic charging effects, we furthermore introduce an offset in the gate voltage of  $-107 \pm 6 \text{ V}$  for  $E_F = 0$ . This value was extrapolated

from the gate dependence of the photoluminescence Stokes shift<sup>21,25</sup> (Supplementary Section S2).

When the Fermi energy is varied from  $\sim 0$  to 30 meV, the exciton energy blue-shifts monotonically, whereas the trion energy remains largely unchanged, after a slight initial redshift (Fig. 2b). These dependences arise from the combined effects of Pauli blocking and many-body interactions<sup>25,26</sup>, and are consistent with the previous theoretical results (Supplementary Section S3) and experimental studies on quantum wells (refs 10–13). The splitting between the exciton and trion energy is predicted to be linearly dependent on the Fermi energy and obey<sup>11</sup>

$$\omega_A - \omega_{A^-} = E_{A^-} + E_F \quad (1)$$

where  $E_{A^-}$  is the trion binding energy. Because the exciton can be considered as an ionized trion,  $\omega_A - \omega_{A^-}$  defines the minimum energy for the removal of one electron from the trion. In the limit of infinitesimal doping, it is just the trion binding energy  $E_{A^-}$ , the energy required to promote one of the electrons in a trion to the conduction band edge. At finite doping densities, an exciton is obtained by dissociation of a trion and placing the extra electron at the Fermi level, all lower conduction band levels being occupied at zero temperature (inset of Fig. 2c). Our experimental result for  $\omega_A - \omega_{A^-}$  agrees very well with equation (1) (Fig. 2c), further confirming the spectroscopic assignment of the exciton and trion features. We also determine the trion binding energy from the linear fit to be  $18.0 \pm 1.5 \text{ meV}$ . This value is compatible with an estimated trion binding energy of  $E_{A^-} \sim 0.1E_A$  (for isotropic 2D semiconductors with equal electron and hole masses<sup>23</sup>) and the calculated exciton binding energy of  $E_A \approx 0.6 \text{ eV}$  (refs 14,27).

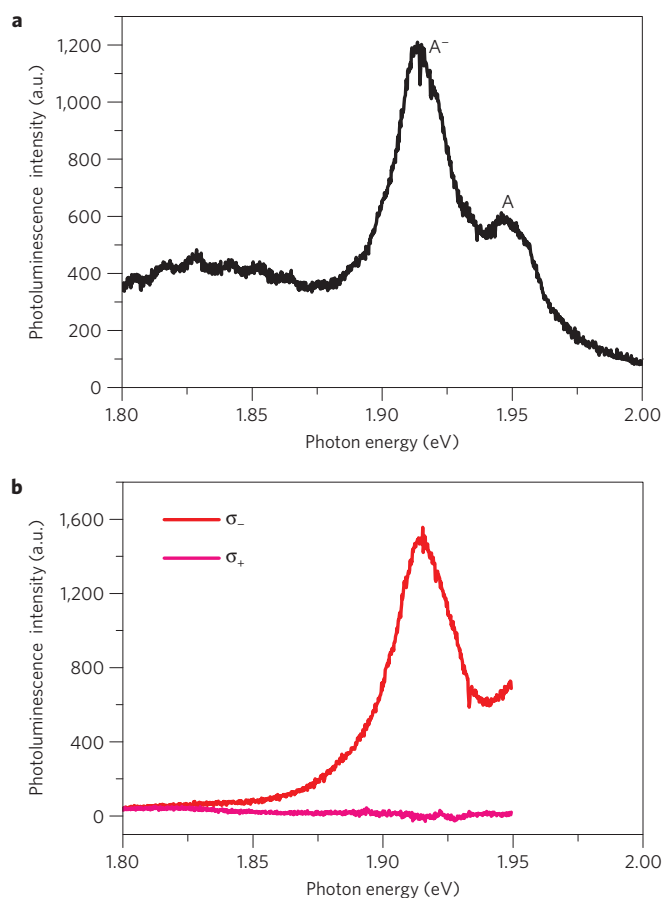


**Figure 4 | Valley and spin control of trions in monolayer MoS<sub>2</sub>.**

**a**, Photoluminescence spectrum of a monolayer MoS<sub>2</sub> sample on a h-BN substrate at 10 K with fully resolved exciton (A) and trion (A<sup>-</sup>) emission. **b**, The left-circularly polarized ( $\sigma_-$ ) and right-circularly polarized ( $\sigma_+$ ) component of the trion emission for excitation by  $\sigma_-$  light at 1.96 eV, nearly on-resonance with the A exciton.

The large trion binding energy observed in monolayer MoS<sub>2</sub> suggests the importance of trions even at elevated temperatures. Indeed, both the exciton and trion features can be identified in the optical response of doped monolayer MoS<sub>2</sub> at room temperature (Fig. 3a,b), although the resonances are significantly broadened. The absorption and especially photoluminescence are highly dependent on doping (Fig. 3c). Whereas the trion photoluminescence is largely gate independent, the exciton photoluminescence varies by nearly two orders of magnitude, which is also correlated with the  $I_{\text{ds}} - V_{\text{g}}$  dependence<sup>12</sup>. This dependence arises primarily from a spectral weight reduction of the exciton resonance with doping, which is consistent with the low-temperature data (although less noticeable at low doping levels owing to the finite temperature effects). The tuning range of the exciton photoluminescence could be further increased with better quality samples. Such strong tunability of the exciton photoluminescence was not observed at 10 K, where emission originates from hot photoluminescence before exciton–trion equilibrium is reached, whereas at room temperature, exciton photoluminescence originates primarily from populations thermally excited from the trion state.

Finally, we demonstrate the unique spin and valley properties of trions in monolayer MoS<sub>2</sub>. Figure 4a shows the photoluminescence spectrum for a monolayer MoS<sub>2</sub> sample on a hexagonal boron nitride (h-BN) substrate at 10 K, where the trion and exciton features are fully resolved because of the high homogeneity of the sample. We optically pump the sample at 1.96 eV, nearly

on-resonance with the A exciton, by left-circularly polarized light ( $\sigma_-$ ). The trion emission is found to be nearly 100% of the same helicity as the pump light (Fig. 4b). Whereas the optical selection rules dictate a single exciton state with hole spin up and electron spin down in the K-valley on absorption of a  $\sigma_-$  photon, multiple trion states are allowed. Among them the lowest energy state consists of hole spin up and two electrons spin down in the K-valley when valley and spin exchange interactions are included. Our photoluminescence result indicates that the optically excited hole in the trion remains spin up, that is, in the K-valley (for a time much longer than the trion lifetime), even in the presence of strong exchange mediated spin relaxation. This suggests the robustness of the hole valley index as a result of the coupled valley and spin degree of freedom<sup>18,22</sup>.

The existence of tightly bound trions with dynamically controllable hole valley and spin in monolayer MoS<sub>2</sub> opens up possibilities of novel many-body phenomena. The large trion binding energy in 2D atomic crystals may also impact the development of new photonic and optoelectronic devices, such as optical detectors or photovoltaic cells. In contrast to neutral excitons, trions can be guided by electric fields, suggesting schemes to overcome the losses associated with the usual diffusive motion of neutral excitons.

## Methods

**Sample preparation.** Monolayer MoS<sub>2</sub> samples were mechanically exfoliated from bulk MoS<sub>2</sub> crystals (SPI) on silicon substrates covered by a 280 nm layer of thermal oxide. Monolayer samples, typically of an area >50  $\mu\text{m}^2$ , were identified by optical microscopy. The sample thickness was confirmed independently by atomic-force microscopy and photoluminescence measurements<sup>2,13</sup>. Monolayer MoS<sub>2</sub> FET devices were fabricated by defining drain and source contacts either through e-beam lithography or photolithography, followed by deposition of Cr/Au or Ni in an e-beam evaporator. For the polarization resolved measurement, the exfoliated samples were transferred to hexagonal boron nitride substrates.

**Optical measurements.** Monolayer MoS<sub>2</sub> FETs were first characterized at 10 K and at room temperature when the back gate was varied systematically from –100 to 80 V. No significant hysteresis was observed. The drain–source current  $I_{\text{ds}}$  was measured in the linear response regime under a drain–source bias voltage  $V_{\text{ds}} = 40$  mV across a channel length of 10  $\mu\text{m}$ . For optical absorption measurements, the broadband radiation from a quartz tungsten halogen source was focused onto monolayer MoS<sub>2</sub> by a 40 $\times$  objective. The reflected radiation was collected and analysed with a grating spectrometer equipped with a liquid nitrogen cooled CCD.

The reflectance contrast was measured by normalizing the radiation reflected from the sample on substrate to that from the bare substrate. The sample absorbance was obtained from the reflectance by using a Kramers–Kronig constrained variational analysis<sup>28</sup> (Supplementary Section S4). Photoluminescence measurements were performed using the same set-up with a single-mode solid-state laser centred at 532 nm. The laser intensity on the sample was kept below 500 W cm<sup>-2</sup>, which corresponds to a steady-state photoexcitation density of  $\sim 10^{10}$  cm<sup>-2</sup> in monolayer MoS<sub>2</sub> (refs 2,29). This is  $\sim 2$ –3 orders of magnitude lower than the electron doping density induced by the silicon back gate. For the polarization resolved measurements, a Babinet–Soleil compensator was used to produce circularly polarized 632.8 nm light from a HeNe laser. Emission from the sample passed through a combination of a quarter-wave Fresnel rhomb and an analyser for selection of the left- and right-circularly polarized components.

**Analysis of the absorption spectra.** We used the predicted single-sided power-law spectral dependence of the exciton and trion absorbance in doped 2D semiconductors,  $A(\omega) = \sum_{X=A,A^-} a_X (\omega - \omega_X)^{-\alpha_X}$  (for  $\omega > \omega_X$ ) (refs 21,24). This expression corresponds to a shake-up process, a non-instantaneous evolution of the 2DEG to a new equilibrium configuration on creation of a hole<sup>21,24</sup>. Here  $a_X$ ,  $\omega_X$  and  $\alpha_X$  are, respectively, the amplitude, threshold energy and critical exponent of resonance  $X$  ( $X = A$  and  $A^-$ ). In the limit of relatively low doping densities, as in our experiment,  $a_X$  ( $X = A, A^-$ ) depend weakly on doping<sup>24</sup> and were kept as constants. To compare with experiment, the power-law dependence was convoluted with a Gaussian to account for sample inhomogeneity and the onset of indirect optical transitions in doped semiconductors<sup>21</sup>. In addition, a smooth background describing the low-energy tail of higher energy transitions was subtracted from experimental spectra. (See Supplementary Sections S3 and S4 for details.) The fits (green lines, Fig. 2a), with individual contributions from excitons and trions (blue lines), are in good agreement with experiment (red lines). At positive gate voltages the exciton absorption is very weak and is omitted from the fitting.

Received 23 July 2012; accepted 30 October 2012;  
published online 2 December 2012

## References

- Novoselov, K. S. Nobel lecture: Graphene: Materials in the Flatland. *Rev. Mod. Phys.* **83**, 837–849 (2011).
- Mak, K. F., Lee, C., Hone, J., Shan, J. & Heinz, T. F. Atomically thin MoS<sub>2</sub>: A new direct-gap semiconductor. *Phys. Rev. Lett.* **105**, 136805 (2010).
- Splendiani, A. *et al.* Emerging photoluminescence in monolayer MoS<sub>2</sub>. *Nano Lett.* **10**, 1271–1275 (2010).
- Li, T. & Galli, G. Electronic properties of MoS<sub>2</sub> nanoparticles. *J. Phys. Chem. C* **111**, 16192–16196 (2007).
- Lebegue, S. & Eriksson, O. Electronic structure of two-dimensional crystals from *ab initio* theory. *Phys. Rev. B* **79**, 115409 (2009).
- Radisavljevic, B., Radenovic, A., Brivio, J., Giacometti, V. & Kis, A. Single-layer MoS<sub>2</sub> transistors. *Nature Nanotech.* **6**, 147–150 (2011).
- Mak, K. F., He, K., Shan, J. & Heinz, T. F. Control of valley polarization in monolayer MoS<sub>2</sub> by optical helicity. *Nature Nanotech.* **7**, 494–498 (2012).
- Zeng, H., Dai, J., Yao, W., Xiao, D. & Cui, X. Valley polarization in MoS<sub>2</sub> monolayers by optical pumping. *Nature Nanotech.* **7**, 490–493 (2012).
- Cao, T. *et al.* Valley-selective circular dichroism of monolayer molybdenum disulphide. *Nature Commun.* **3**, 887 (2012).
- Kheng, K. *et al.* Observation of negatively charged excitons X<sup>-</sup> in semiconductor quantum wells. *Phys. Rev. Lett.* **71**, 1752–1755 (1993).
- Huard, V., Cox, R. T., Saminadayar, K., Arnoult, A. & Tatarenko, S. Bound states in optical absorption of semiconductor quantum wells containing a two-dimensional electron gas. *Phys. Rev. Lett.* **84**, 187–190 (2000).
- Finkelstein, G., Shtrikman, H. & Bar-Joseph, I. Optical spectroscopy of a two-dimensional electron gas near the metal-insulator transition. *Phys. Rev. Lett.* **74**, 976–979 (1995).
- Lee, C. *et al.* Anomalous lattice vibrations of single- and few-layer MoS<sub>2</sub>. *ACS Nano* **4**, 2695–2700 (2010).
- Cheiwchanamngij, T. & Lambrecht, W. R. L. Quasiparticle band structure calculation of monolayer, bilayer, and bulk MoS<sub>2</sub>. *Phys. Rev. B* **85**, 205302 (2012).
- Spivak, B., Kravchenko, S. V., Kivelson, S. A. & Gao, X. P. A. Colloquium: Transport in strongly correlated two dimensional electron fluids. *Rev. Mod. Phys.* **82**, 1743–1766 (2010).
- Wigner, E. On the interaction of electrons in metals. *Phys. Rev.* **46**, 1002–1011 (1934).
- Mattheiss, L. F. Band structures of transition-metal-dichalcogenide layer compounds. *Phys. Rev. B* **8**, 3719–3740 (1973).
- Xiao, D., Liu, G.-B., Feng, W., Xu, X. & Yao, W. Coupled spin and valley physics in monolayers of MoS<sub>2</sub> and other group-VI dichalcogenides. *Phys. Rev. Lett.* **108**, 196802 (2012).
- Ayari, A., Cobas, E., Ogundadegbe, O. & Fuhrer, M. S. Realization and electrical characterization of ultrathin crystals of layered transition-metal dichalcogenides. *J. Appl. Phys.* **101**, 014507 (2007).
- Evans, B. L. & Young, P. A. Optical absorption and dispersion in molybdenum disulphide. *Proc. R. Soc. Lond. A* **284**, 402 (1965).
- Ruckenstein, A. E. & Schmitt-Rink, S. Many-body aspects of the optical spectra of bulk and low-dimensional doped semiconductors. *Phys. Rev. B* **35**, 7551–7557 (1987).
- Stebe, B. & Aïnane, A. Ground-state energy and optical-absorption of excitonic trions in two-dimensional semiconductors. *Superlattices Microstruct.* **5**, 545–548 (1989).
- Thilagam, A. Two-dimensional charged-exciton complexes. *Phys. Rev. B* **55**, 7804–7808 (1997).
- Ohtaka, K. & Tanabe, Y. Theory of the soft-X-ray edge problem in simple metals: Historical survey and recent developments. *Rev. Mod. Phys.* **62**, 929–991 (1990).
- Hawrylak, P. Optical properties of a two-dimensional electron gas: Evolution of spectra from excitons to Fermi-edge singularities. *Phys. Rev. B* **44**, 3821–3828 (1991).
- Ogawa, T. Quantum states and optical responses of low-dimensional electron-hole systems. *J. Phys. Condens. Matter* **16**, S3567–S3595 (2004).
- Ramasubramaniam, A. Large excitonic effects in monolayers of molybdenum and tungsten dichalcogenides. *Phys. Rev. B* **86**, 115409 (2012).
- Kuzmenko, A. B. Kramers-Kronig constrained variational analysis of optical spectra. *Rev. Scient. Inst.* **76**, 083108 (2005).
- Korn, T., Heydrich, S., Hirmer, M., Schmutzler, J. & Schueller, C. Low-temperature photocarrier dynamics in monolayer MoS<sub>2</sub>. *Appl. Phys. Lett.* **99**, 102109 (2011).

## Acknowledgements

This research was supported by the National Science Foundation through grants DMR-0907477 and the Research Corporation Scialog Program at Case Western Reserve University; and by the National Science Foundation through grants DMR-1106172 and 1122594 and by the Department of Energy, Office of Basic Energy Sciences through grant DE-FG02-07ER15842 at Columbia University and through grant DE-SC0001085 for optical instrumentation at Columbia University's Center for Re-Defining Photovoltaic Efficiency through Molecule Scale Control. C.L. acknowledges support from the Korean government Ministry of Education grant Global Frontier Research Center for Advanced Soft Electronics (2011-0031629), and G.H.L. support from Samsung-SKKU Graphene Center.

## Author contributions

K.F.M. and J.S. designed the experiment, performed the measurement and analysis, and prepared the manuscript; K.H. fabricated MoS<sub>2</sub> FET devices and measured photoluminescence; C.L. and J.H. developed MoS<sub>2</sub> FET devices; G.H.L. fabricated MoS<sub>2</sub> samples on BN; T.F.H. contributed to the interpretation of the results and writing of the manuscript.

## Additional information

Supplementary information is available in the online version of the paper. Reprints and permissions information is available online at [www.nature.com/reprints](http://www.nature.com/reprints). Correspondence and requests for materials should be addressed to J.S.

## Competing financial interests

The authors declare no competing financial interests.